Pergamon

Int. J. Solids Structures Vol. 35, Nos 28–29, pp. 3831–3853, 1998

0020–7683/98 $19.00 + .00

PII: S0020–7683(97)00221–7

TWO-DIMENSIONAL DYNAMIC AND THREE-DIMENSIONAL FRACTURE IN VISCOELASTIC MATERIALS

M. J. DANYLUK,† P. H. GEUBELLE* and H. H. HILTON
Department of Aeronautical and Astronautical Engineering, University of Illinois at Urbana-Champaign, IL, U.S.A.

(*Received* 1 *May* 1997; *in revised form* 22 *July* 1997)

Abstract—This paper presents a numerical scheme specially developed for 2-D and 3-D viscoelastodynamic fracture problems. The method, referred to as the spectral scheme, is derived from a spectral form of the viscoelastodynamic boundary integral relation between the traction stresses acting on the fracture plane and the corresponding displacement discontinuities. It accommodates planar cracks of arbitrary shapes embedded in an infinite homogeneous viscoelastic medium and subjected to an arbitrary combination of time- and space-varying tensile and shear loading. A wide range of cohesive models can be incorporated to characterize the failure process taking place in the vicinity of the spontaneously propagating crack tip. Various viscoelastic dynamic fracture problems involving stationary and spontaneously propagating cracks are presented, including a study of the material-induced dissipative effect on the propagation of transient surface waves, and an investigation of the effects of a simple rate-dependent cohesive failure model on spontaneous crack propagation in elastic and viscoelastic materials.

1. INTRODUCTION

Due to the complexity of the constitutive relations needed to capture the time-dependent response and failure process of viscoelastic materials, numerical techniques are often required to investigate the failure mechanics of this class of materials. Among the computational methods used for viscoelastic fracture problems, the finite element method (FEM) is the most common (Warby *et al.*, 1992; Masuero and Creus, 1993; Duong and Knauss, 1995) but seems to have been used mainly in quasi-static situations. Another type of numerical technique has been recently introduced by Georgiadis and co-workers (1991), Georgiadis (1993) to investigate a series of dynamic fracture problems involving cracks embedded in a viscoelastic medium. Their method, which is based on a combination of integral transforms and numerical Laplace inversions, has been used to determine viscoelastic effects on the dynamic stress intensity factor associated with sudden loading of non-moving cracks in simple geometrical settings (linear or penny-shape cracks).

The objective of this work is to develop and implement an efficient numerical scheme able to accurately simulate a wide range of 2-D and 3-D viscoelastodynamic fracture problems involving planar stationary or spontaneously propagating cracks of arbitrary shapes subjected to arbitrary space- and time-varying loading conditions. The spectral method described hereafter is a special form of the viscoelastodynamic boundary integral relation between the stresses and the displacement appearing on the fracture plane. It is based on a 3-D spectral formulation obtained by Geubelle and Rice (1995) in the linearly elastic case. While conceptually similar, the elastic and viscoelastic spectral schemes present some important differences which have been emphasized in a recent paper by Geubelle *et al.* (1998) in the simpler scalar framework of anti-plane shear (Mode III) loading. That preliminary paper, which also provides a review of previous analytical work on viscoelastodynamic fracture mechanics, is now extended to 2-D in-plane (Modes I and II) and fully 3-D situations.

* Author to whom correspondence should be addressed.
† Current address: GE Research Center, Schenectady, NY.

The present paper is organized as follows: The spectral formulation is first summarized in Section 2. Then, the classical 2-D problem of a tensile line load suddenly applied on a viscoelastic half space is solved in Section 3 to illustrate the material-induced dissipative effect on the propagation of transient surface waves. In Section 4, the spectral method is used to simulate sudden Mode I loadings of 2-D and 3-D stationary cracks in a standard linear viscoelastic solid. Finally, a simple rate-dependent cohesive model is used in the simulation of spontaneously propagating and arresting 2-D tensile cracks in Section 5.

2. FORMULATION OF THE VISCOELASTODYNAMIC SPECTRAL SCHEME

The spectral scheme described in this paper has been developed to investigate fracture problems similar to that schematically represented in Fig. 1. A planar crack or fault of arbitrary shape occupies a portion of the plane $x_2 = 0$ (referred to as the fracture plane) and is embedded in an infinite homogeneous viscoelastic medium, the constitutive relations of which can be expressed in the conventional differential form:

$$\sigma_{ij} = \lambda_0 \mathscr{N}(D)\varepsilon_{kk}\delta_{ij} + 2\mu_0 \mathscr{M}(D)\varepsilon_{ij}, \tag{1}$$

where σ_{ij} and ε_{ij} are the stresses and infinitesimal strains, respectively; $\mathscr{N}$ and $\mathscr{M}$ are nondimensional ratios of differential operator sums containing various orders of $D = \partial/\partial t$; λ_0 and μ_0 are the (instantaneous) elastic Lamé constants; δ_{ij} is the Kronecker delta. Under the effect of arbitrary space- and time-varying tensile and/or shear loads, the crack expands spontaneously on its original plane.

As mentioned earlier, the spectral scheme consists in a special form of the boundary integral formulation of the viscoelastodynamic relations between the traction stresses $\tau_j(x_1, x_3, t) = \sigma_{2j}(x_1, x_2 = 0, x_3, t)$ acting on the fracture plane and the corresponding displacement discontinuities (or crack opening displacement COD) $\delta_j(x_1, x_3, t)$ defined as

$$\delta_j(x_1, x_3, t) = u_j(x_1, x_2 = 0^+, x_3, t) - u_j(x_1, x_2 = 0^-, x_3, t),$$

where u_j denote the displacement components. The final form of the viscoelastodynamic relations to be derived hereafter will be somewhat different from that obtained in the linearly elastic situation (Geubelle and Rice, 1995) and will be written as

$$\tau_j(x_1, x_3, t) = \tau_j^0(x_1, x_3, t) - V_{jk}\dot{\delta}_k(x_1, x_3, t) + W_{jk}\delta_k(x_1, x_3, t) + f_j(x_1, x_3, t),$$

where τ_j^0 are externally applied traction stresses and the dot denotes differentiation with

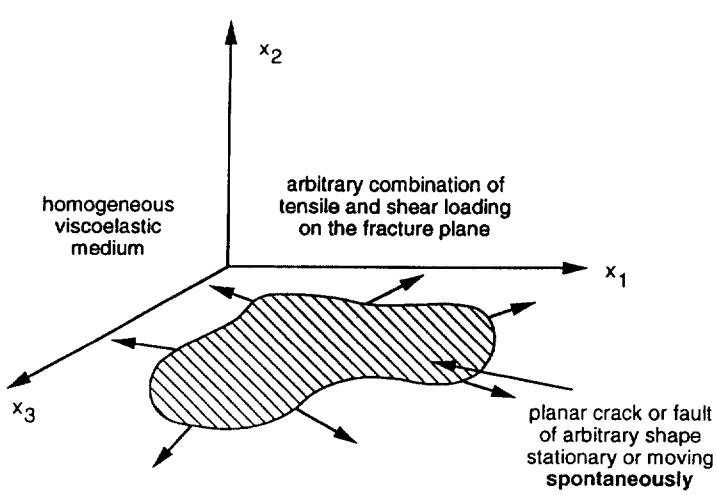

Fig. 1. Geometry of the 3-D elastodynamic fracture problem.

respect to time. The term $V_{jk}\dot{\delta}_k$ corresponds to the instantaneous "radiation" term and involves the instantaneous (elastic) properties of the material. The next term ($W_{jk}\delta_k$) is characteristic of the viscoelastic problem and vanishes in the elastic limit. Finally, f_j is the convolution term which will be expressed in the spectral (Fourier) domain as a time convolution over the past crack opening displacement (COD) history. The convolution term will account for both the elastodynamic and viscoelastic hereditary effects and will be quite different from its elastic counterpart. The fundamental differences between the two cases are similar to those emphasized in the simpler 2-D Mode III case (Geubelle *et al.*, 1998) and involve a strong dependence of the convolution on the spectral mode number, especially in the vicinity of the origin, and a non-vanishing contribution of the constant spectral mode to the convolution. Following the procedure used in the elastic situation, we start by considering the two 2-D in-plane fracture modes (Modes I and II) before moving on to the fully 3-D problem. Since the derivation steps are somewhat similar to those described in Geubelle and Rice (1995) for the elastic problem, the following presentation is limited to the most essential relations.

2.1. *Two-dimensional in-plane fracture modes*

We first assume that the solution is independent of x_3. The in-plane displacement components $u_\alpha(x_\beta, t)$ can be expressed as

$$u_1(x_\beta, t) = \phi_{,1}(x_\beta, t) + \psi_{,2}(x_\beta, t), \quad u_2(x_\beta, t) = \phi_{,2}(x_\beta, t) - \psi_{,1}(x_\beta, t),$$

where the potentials ϕ and ψ satisfy the equations

$$[c_d(D)]^2 \phi_{,\alpha\alpha} = \ddot{\phi}, \quad [c_s(D)]^2 \psi_{,\alpha\alpha} = \ddot{\psi}, \tag{2}$$

in which

$$[c_d(D)]^2 = \frac{\lambda_0 \mathcal{N}(D) + 2\mu_0 \mathcal{M}(D)}{\rho} = c_{d0}^2 \mathcal{Q}(D), \quad [c_s(D)]^2 = \frac{\mu_0 \mathcal{M}(D)}{\rho} = c_{s0}^2 \mathcal{M}(D). \tag{3}$$

In (3), ρ is the density; $c_{d0} = ((\lambda_0 + 2\mu_0)/\rho)^{1/2}$ and $c_{s0} = (\mu_0/\rho)^{1/2}$ are the elastic (instantaneous) dilatational and shear wave speeds, respectively; $\mathcal{Q}(D)$ is a linear combination of $\mathcal{M}$ and $\mathcal{N}$, the two nondimensional ratios of differential operators introduced in (1):

$$\mathcal{Q}(D) = \frac{\lambda_0}{\lambda_0 + 2\mu_0} \mathcal{N}(D) + \frac{2\mu_0}{\lambda_0 + 2\mu_0} \mathcal{M}(D). \tag{4}$$

To solve the viscoelastic wave eqns (2), we consider a particular spectral term:

$$[\phi(x_\alpha, t), \psi(x_\alpha, t)] = e^{iqx_1} [\Phi(x_2, t; q), \Psi(x_2, t; q)],$$

and take the Laplace transform of the Fourier coefficients, as in

$$\hat{\Phi}(x_2, p; q) = \int_0^\infty e^{-pt} \Phi(x_2, t; q)\, \mathrm{d}t.$$

Substitution into (2) yields

$$\frac{\mathrm{d}^2}{\mathrm{d}x_2^2} \hat{\Phi}(x_2, p; q) = q^2 \hat{\alpha}_d(p; q) \hat{\Phi}(x_2, p; q), \quad \frac{\mathrm{d}^2}{\mathrm{d}x_2^2} \hat{\Psi}(x_2, p; q) = q^2 \hat{\alpha}_s(p; q) \hat{\Psi}(x_2, p; q),$$

where

$$\hat{\alpha}_d(p;q) = \sqrt{1+\frac{p^2}{q^2\hat{c}_d(p)}}, \quad \hat{\alpha}_s(p;q) = \sqrt{1+\frac{p^2}{q^2\hat{c}_s(p)}}.$$

In the latter, the complex square root is chosen to have a non-negative real part, while $\hat{c}_d(p)$ and $\hat{c}_s(p)$ are the Laplace transforms of the dilatational and shear wave speeds, respectively:

$$\hat{c}_d(p) = c_{d0}(\hat{\mathscr{Q}}(p))^{1/2}, \quad \hat{c}_s(p) = c_{s0}(\hat{\mathscr{M}}(p))^{1/2}. \tag{5}$$

The time dependences of the wave speeds are the main difference between the derivation of the spectral formulation in the viscoelastic and elastic cases. The remaining initial steps are similar, and lead to the following relations between the traction stresses on the fracture plane and the associated displacement discontinuities (see Geubelle and Rice, 1995 for details):

$$\hat{T}_1(p;q) = -\frac{\mu_0\hat{\mathscr{M}}(p)}{2}\left[\frac{4\hat{\alpha}_s(p;q)\hat{\alpha}_d(p;q)-(1+\hat{\alpha}_s^2(p;q))^2}{\hat{\alpha}_s(p;q)(1-\hat{\alpha}_s^2(p;q))}\right]\hat{D}_1(p;q),$$

$$\hat{T}_2(p;q) = -\frac{\mu_0\hat{\mathscr{M}}(p)}{2}\left[\frac{4\hat{\alpha}_s(p;q)\hat{\alpha}_d(p;q)-(1+\hat{\alpha}_s^2(p;q))^2}{\hat{\alpha}_d(p;q)(1-\hat{\alpha}_s^2(p;q))}\right]\hat{D}_2(p;q), \tag{6}$$

where $T_\alpha(t;q)$ and $D_\alpha(t;q)$ are the Fourier coefficients of the traction stresses and crack opening displacements, respectively, defined by

$$[\tau_\alpha(x_1,t),\delta_\alpha(x_1,t)] = [T_\alpha(t;q),D_\alpha(t;q)]\,e^{iqx_1}.$$

At this point, we extract the instantaneous response:

$$[\tau_1(x_1,t)]_{\text{inst}} = -\frac{\mu_0}{2c_{s0}}\delta_1(x_1,t), [\tau_2(x_1,t)]_{\text{inst}} = -\frac{\lambda_0+2\mu_0}{2c_{d0}}\dot{\delta}_2(x_1,t) = -\frac{\mu_0}{2c_{s0}}\frac{c_{d0}}{c_{s0}}\dot{\delta}_2(x_1,t),$$

which, in the Laplace/Fourier domain, transforms (6) into

$$\hat{T}_1 = -\frac{\mu_0}{2c_{s0}}p\hat{D}_1 - \frac{\mu_0|q|}{2}\left[\frac{4\hat{\alpha}_s\hat{\alpha}_d-(1+\hat{\alpha}_s^2)^2}{\hat{\alpha}_s(1-\hat{\alpha}_s^2)}\hat{\mathscr{M}}-\frac{p}{|q|c_{s0}}\right]\hat{D}_1,$$

$$\hat{T}_2 = -\frac{\mu_0}{2c_{s0}}\frac{c_{d0}}{c_{s0}}p\hat{D}_2 - \frac{\mu_0|q|}{2}\left[\frac{4\hat{\alpha}_s\hat{\alpha}_d-(1+\hat{\alpha}_s^2)^2}{\hat{\alpha}_d(1-\hat{\alpha}_s^2)}\hat{\mathscr{M}}-\frac{p}{|q|c_{s0}}\frac{c_{d0}}{c_{s0}}\right]\hat{D}_2. \tag{7}$$

Back in the time domain, the latter yield

$$\tau_1(x_1,t) = \tau_1^0(x_1,t) - \frac{\mu_0}{2c_{s0}}\dot{\delta}_1(x_1,t) + \bar{f}_1(x_1,t),$$

$$\tau_2(x_1,t) = \tau_2^0(x_1,t) - \frac{c_{d0}}{c_{s0}}\frac{\mu_0}{2c_{s0}}\dot{\delta}_2(x_1,t) + \bar{f}_2(x_1,t), \tag{8}$$

where the externally applied stresses τ_α^0 have been added. The convolution term $\bar{f}_\alpha$ are expressed in the Fourier domain as

$$\bar{F}_\alpha(t;q) = -\frac{\mu_0|q|}{2}\int_{-\infty}^{t} R_\alpha^{VE}(|q|c_{s0}t')D_\alpha(t-t';q)|q|c_{s0}\,dt', \quad \text{(no sum on } \alpha) \tag{9}$$

where the convolution kernels $R_\alpha^{VE}(T)$ are the inverse Laplace transforms of the square-bracketed terms in (7) written in terms of the nondimensional variable $s = p/(|q|c_{s0})$.

Unlike in the elastic case, the convolution kernel $R_\alpha^{VE}(T)$ has a nonvanishing limit for large values of s in the Laplace domain, and, to adequately capture the behavior of the convolution kernel at the origin, we must define an alternative form of the kernel $C_\alpha^{VE}(T)$ by

$$\hat{C}_\alpha^{VE}(s) = \hat{R}_\alpha^{VE}(s) - \lim_{s\to\infty}[\hat{R}_\alpha^{VE}(s)] = \hat{R}_\alpha^{VE}(s) - R_\alpha^{\infty}.$$

Equation (9) then becomes (no sum on α)

$$\bar{F}_\alpha(t;q) = -\frac{\mu_0|q|}{2}R_\alpha^{\infty}D_\alpha(t;q) - \frac{\mu_0|q|}{2}\int_{-\infty}^{t} C_\alpha^{VE}(|q|c_{s0}t')D_\alpha(t-t';q)|q|c_{s0}\,dt'.$$

As will become apparent later, R_α^{∞} is inversely proportional to $|q|c_{s0}\tilde{\tau}^*$, where $\tilde{\tau}^*$ is the reference relaxation time parameter characterizing the time dependence of the viscoelastic material, and the proportionality factor depends on the material model used. $C_1^{VE}(T)$ $(= C_{II}^{VE}(T))$ and $C_2^{VE}(T)$ $(= C_I^{VE}(T))$ constitute the Mode II and Mode I viscoelastodynamic convolution kernels for the spectral scheme, respectively. The presence of the non-dimensional viscoelastic response operators $\mathscr{M}$ and $\mathscr{N}$ [explicitly and through $\hat{\alpha}_d$ and $\hat{\alpha}_s$ in (7)] render the Laplace domain expression of the kernels very complicated. For most cases, the inversion must be preformed numerically using, for example, the DAC technique (Dubner and Abate, 1968; Crump, 1976).

In the remainder of this presentation, we will focus on the simple Standard Linear Solid (SLS) model for which

$$\hat{\mathscr{M}}(p) = \frac{p+1/\tilde{\tau}}{p+(1+\xi)/\tilde{\tau}} = \hat{\mathscr{N}}(p), \tag{10}$$

where $\tilde{\tau}$ is the unique relaxation time parameter, and $\xi = \mu_0/\mu_\infty - 1$ characterizes the change in elastic properties from the instantaneous shear modulus μ_0 to the fully relaxed value μ_∞. This model, which assumes the moduli to be synchronous (i.e., Poisson's ratio ν is constant), is clearly oversimplified (Hilton, 1996; Hilton and Yi, 1997). It is, however, particularly attractive in a preliminary investigation of the viscoelastic effects by qualitatively capturing a wide range of phenomena with the aid of only two parameters ($\tilde{\tau}$ and ξ). The spectral formulation in the more general situation involving a Prony series representation of the material response is presented in Appendix A.

For the SLS class of materials, the convolution kernels take the form $C_\alpha^{VE} = C_\alpha^{VE}(T;b,\xi,h)$ where $b = 1/|q|c_{s0}\tilde{\tau}$ and $h = c_{d0}/c_{s0} = \sqrt{2(1-\nu)/(1-2\nu)}$. In other words, the dependence of the convolution kernels on the time constant $\tilde{\tau}$, which is a main characteristic of the viscoelastodynamic spectral formulation, can be cast in the nondimensional parameter b. The Laplace domain expressions of the convolution kernels C_α^{VE} for the SLS model are given in Appendix B and the kernels are presented in the time domain in Fig. 2(a–d) for two values of ξ and for $h = \sqrt{3}$ (which corresponds to $\nu = 0.25$).

The basic characteristics of the Mode I and II kernels are similar to those observed for the Mode III kernel (Geubelle *et al.*, 1998). As b becomes very small, the viscoelastic convolution kernels C_α^{VE} approach their elastic counterparts C_α^{EL} derived in Geubelle and Rice (1995) as

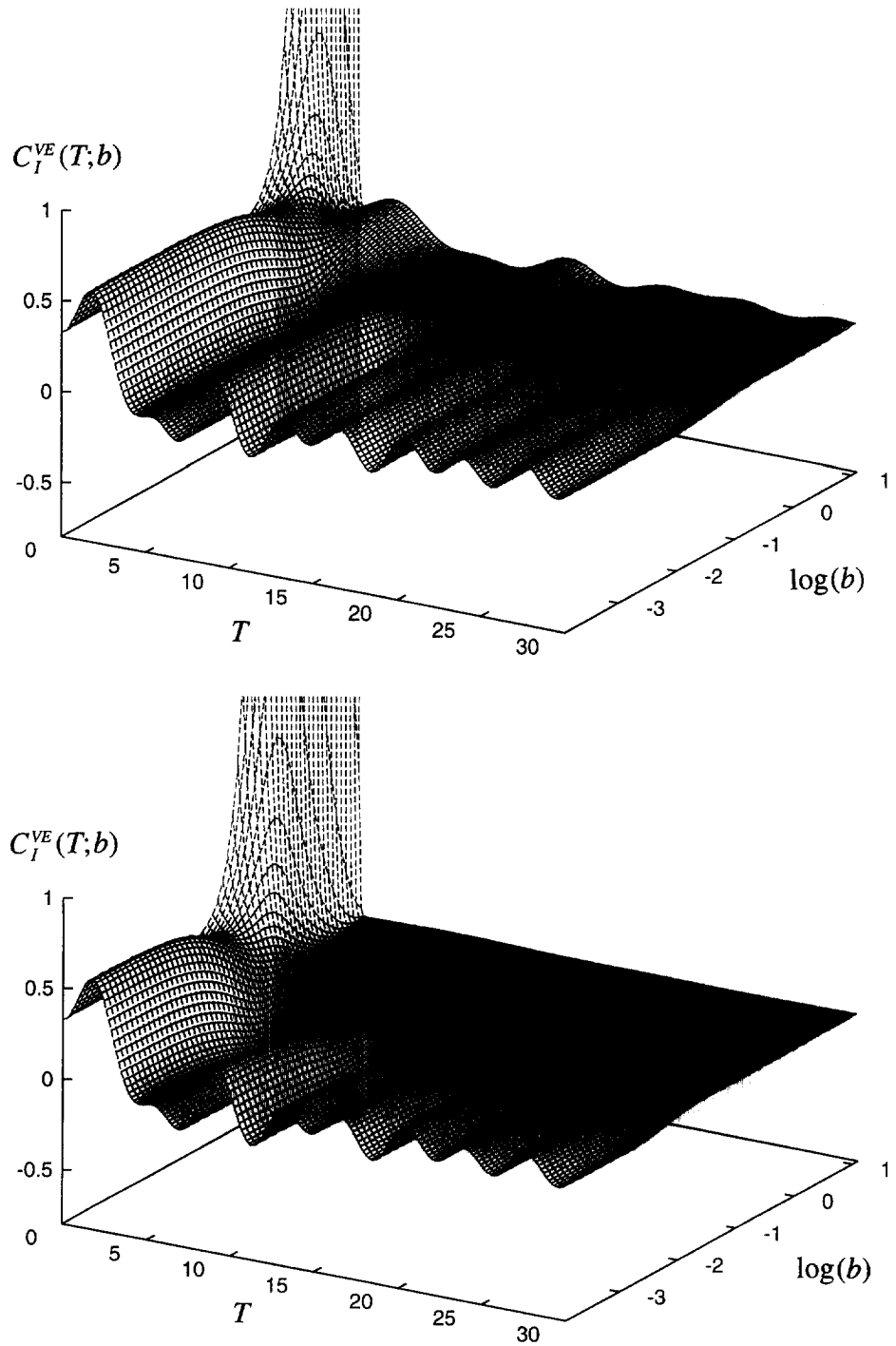

Fig. 2. Viscoelastodynamic convolution kernel: (a) Mode I kernel for $\xi = 1$; (b) Mode I kernel for $\xi = 10$; (c) Mode II kernel for $\xi = 1$; (d) Mode II kernel for $\xi = 10$.

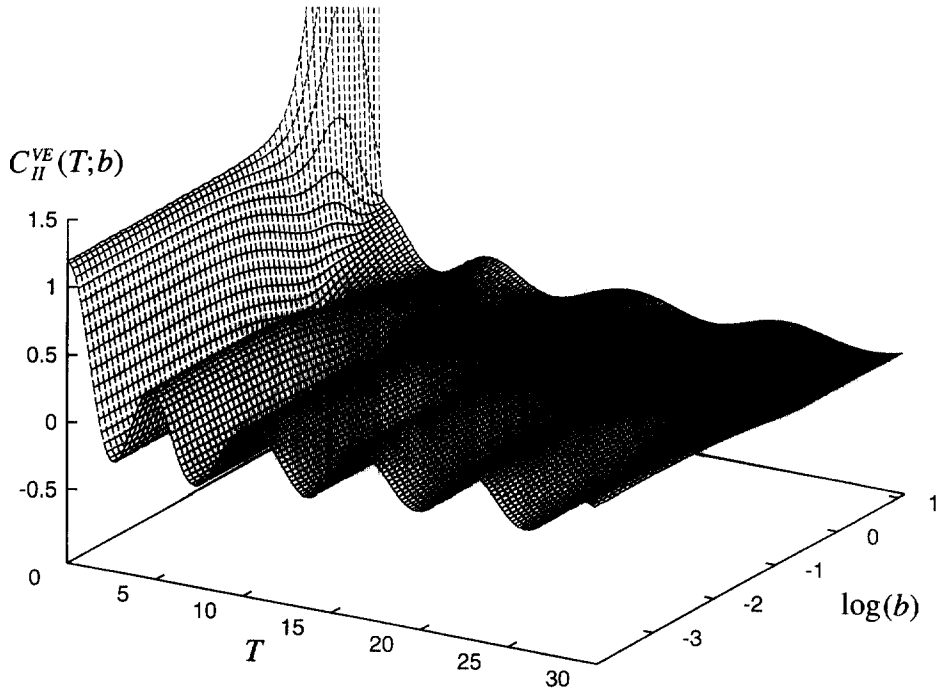

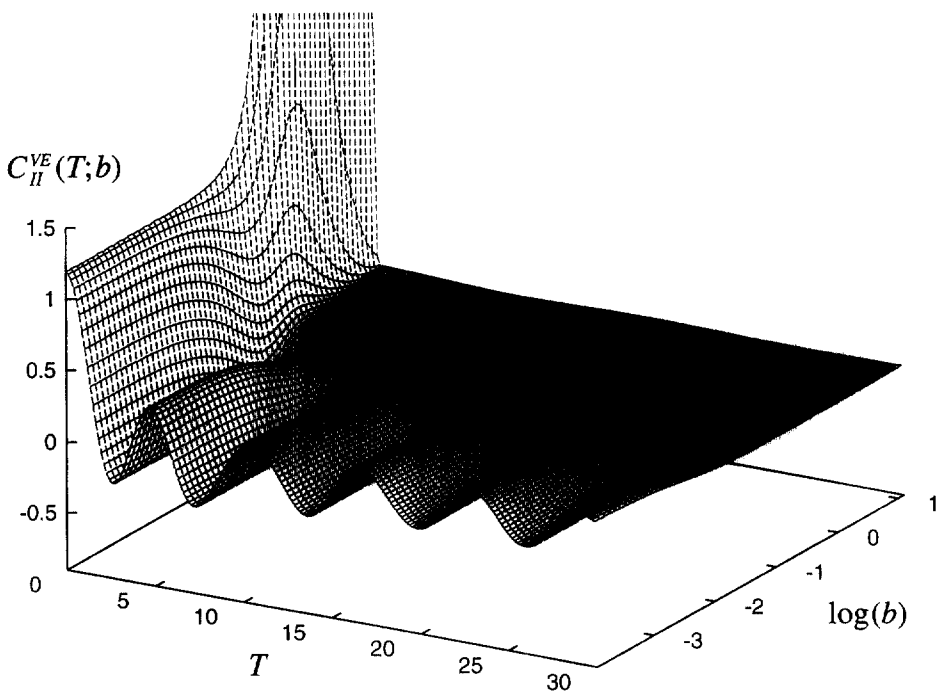

Fig. 2.—*Continued.*

$$\lim_{b\to 0} C_{\mathrm{I}}^{VE}(T;b,\xi,h) = C_{I}^{EL}(T;h)$$

$$= h^2\frac{J_1(hT)}{T} + 4T[W(T) - W(hT)] + (4h - h^3)J_0(hT) - 4J_0(T),$$

$$\lim_{b\to 0} C_{\mathrm{II}}^{VE}(T;b,\xi,h) = C_{\mathrm{II}}^{EL}(T;h)$$

$$= \frac{J_1(T)}{T} + 4T[W(hT) - W(T)] - \frac{4}{h}J_0(hT) + 3J_0(T),$$

where J_0 and J_1 are Bessel functions and $W(T) = 1 - \int_0^T J_1(x)/x\,\mathrm{d}x$. Also, just as in the Mode III case, for large values of b, the kernels show a severe drop near the origin $T = 0$, where they take the value

$$C_{\mathrm{I}}^{VE}(T=0;b,\xi,h) = hb^2\xi\left(\frac{3\xi}{8} + \frac{1}{2}\right) + \frac{(8-h^2)h}{2} - 4,$$

$$C_{\mathrm{II}}^{VE}(T=0;b,\xi,h) = b^2\xi\left(\frac{3\xi}{8} + \frac{1}{2}\right) + \frac{7}{2} - \frac{4}{h}.$$

The value at the origin becomes unbounded as $b \to \infty$, i.e., as $\tilde{\tau}$ and/or q tend to zero. This requires special treatment of the constant mode ($q = 0$) which, unlike in the elastic case, contributes to the convolution term. Following the procedure used in Geubelle *et al.* (1996), the constant (or zeroth) spectral mode contribution to the term $\bar{f}_\alpha$ in (8) is expressed as

$$\bar{F}_1(t;0) = \frac{\mu_0\xi}{4c_{s0}\tilde{\tau}}D_1(t;0) - \frac{\mu_0}{2c_{s0}\tilde{\tau}}\int_0^t C_0^{VE}\left(\frac{t'}{\tilde{\tau}}\right)D_1(t-t';0)\frac{\mathrm{d}t'}{\tilde{\tau}},$$

$$\bar{F}_2(t;0) = \frac{h\mu_0\xi}{4c_{s0}\tilde{\tau}}D_2(t;0) - \frac{h\mu_0}{2c_{s0}\tilde{\tau}}\int_0^t C_0^{VE}\left(\frac{t'}{\tilde{\tau}}\right)D_2(t-t';0)\frac{\mathrm{d}t'}{\tilde{\tau}},$$

where the constant mode convolution kernel, given by

$$C_0^{VE}(T) = \frac{\xi}{2}e^{-\left(1+\frac{\xi}{2}\right)T}\left[(1+\xi)\left\{I_0\left(\frac{\xi T}{2}\right) - I_1\left(\frac{\xi T}{2}\right)\right\} - \frac{I_1(\xi T/2)}{T}\right], \tag{11}$$

is the same for all three fracture modes and is shown in Fig. 3 for different values of ξ.

Recalling at this point the anti-plane shear formulation obtained in Geubelle *et al.* (1998), we can summarize the 2-D viscoelastodynamic spectral formulation for the SLS class of materials as

$$\tau_j(x_1,t) = \tau_j^0(x_1,t) - V_{jk}\dot{\delta}_k(x_1,t) + W_{jk}\delta_k(x_1,t) + f_j(x_1,t), \tag{12}$$

where V_{jk} and W_{jk} are diagonal matrices:

$$[V_{ij}] = \frac{\mu_0}{2c_{s0}}\mathrm{diag}\,[1,h,1], \quad [W_{ij}] = \frac{\mu_0\xi}{4c_{s0}\tilde{\tau}}\mathrm{diag}\,[1,h,1], \tag{13}$$

and where the remaining convolution terms $f_j(x_1,t)$ are expressed in the Fourier domain as

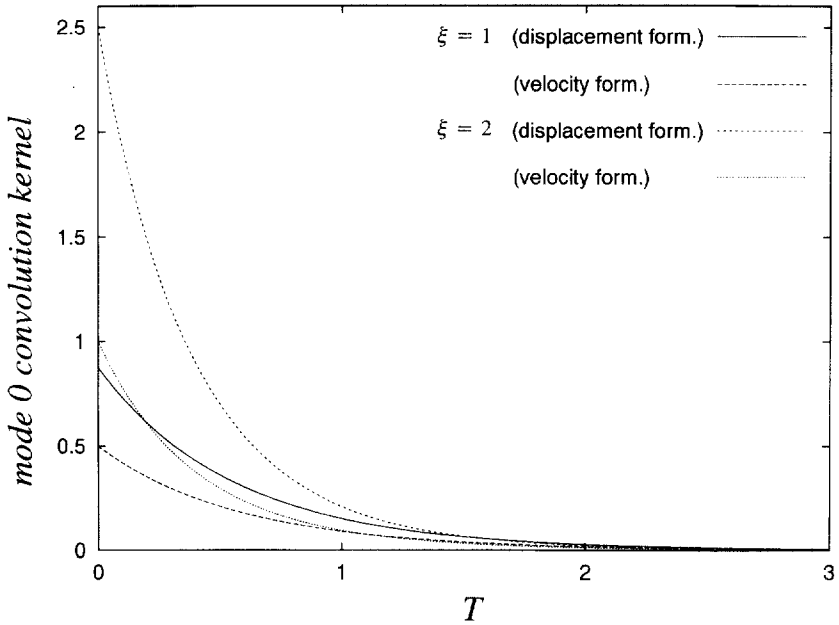

Fig. 3. Constant mode convolution kernel for the displacement and velocity formulations, for two values of ξ.

$$F_j(t;q) = -\frac{\mu_0|q|}{2}\int_{-\infty}^{t} C_j^{VE}(|q|c_{s0}t')D_j(t-t';q)|q|c_{s0}\,\mathrm{d}t',$$

$$F_j(t;0) = -h_j\frac{\mu_0}{2c_{s0}\tilde{\tau}}\int_{-\infty}^{t} C_0^{VE}\left(\frac{t'}{\tilde{\tau}}\right)D_j(t-t';0)\frac{\mathrm{d}t'}{\tilde{\tau}}. \qquad \text{(no sum on } j\text{)} \qquad (14)$$

In the latter, $h_1 = h_3 = 1$, $h_2 = h = c_{d0}/c_{s0}$. The convolution kernels for the non-zero spectral modes are obtained by inverting the Laplace transform expressions listed in Appendix B, while the constant mode kernel is given by (11). It is worth noting once again that both the additional term $W_{jk}\delta_k$ appearing in (12) and the constant mode convolution contribution $F_j(t;0)$ in (14) vanish in the elastic limit for which $\xi \to 0$ and/or $\tilde{\tau} \to \infty$.

The spectral formulation (12)–(14) involves a convolution over the past displacement history and is, therefore, referred to as the displacement formulation. An equivalent expression can be obtained that is based on a convolution over the past velocity history. The so-called velocity formulation is derived by integrating (14) by parts to yield

$$\tau_j(x_1,t) = \tau_j^0(x_1,t) - V_{jk}\dot{\delta}_k(x_1,t) + g_j(x_1,t), \qquad (15)$$

where the convolution term g_j is now expressed in the Fourier domain as

$$G_j(t;q) = -\frac{\mu_0|q|}{2}r_jD_j(t;q) + \frac{\mu_0|q|}{2}\int_0^t W_j^{VE}(|q|c_{s0}t')\dot{D}_j(t-t';q)\,\mathrm{d}t',$$

$$G_j(t;0) = h_j\frac{\mu_0}{2c_{s0}\tilde{\tau}}\int_0^t W_0^{VE}\left(\frac{t'}{\tilde{\tau}}\right)\dot{D}_j(t-t';0)\,\mathrm{d}t', \qquad \text{(no sum on } j\text{)} \qquad (16)$$

with

$$W_j^{VE}(T) = \int_T^{\infty} C_j^{VE}(T')\,\mathrm{d}T',$$

$$W_0^{VE}(T) = \frac{\xi}{2} e^{-\left(1+\frac{\xi}{2}\right)T}\left\{I_0\left(\frac{\xi T}{2}\right) - I_1\left(\frac{\xi T}{2}\right)\right\},$$

and

$$r_1 = r_2 = \frac{2}{\xi+1}\left(1-\frac{1}{h^2}\right), \quad r_3 = \frac{1}{1+\xi}.$$

The convolution kernel for the constant mode $W_0^{VE}(T)$ is represented in Fig. 3 for two values of ξ. It is worth noting that the additional term $W_{jk}\delta_k$ appearing in the viscoelastodynamic displacement-based spectral formulation (12) disappears from the velocity-based relation (15). Note also that the term extracted from the convolution integral in (16a) corresponds to the static long-time limit based on the fully relaxed material properties (recall that $\mu_0/(1+\xi) = \mu_\infty$).

The remainder of this section describes the 3-D formulation for the displacement-based spectral scheme; similar relations can be obtained for the corresponding 3-D velocity formulation.

2.2. *Three-dimensional formulation*

As described in Geubelle and Rice (1995), the 3-D spectral formulation used to solve dynamic fracture problems similar to that depicted in Fig. 1 can easily be derived from the 2-D case by reinstating the x_3-dependence of the variables and by replacing the mode number q in (2.14) by a mode vector $\mathbf{q} = (k, m)$ spanning the fracture plane:

$$[\delta_j(x_1, x_3, t), \tau_j(x_1, x_3, t), f_j(x_1, x_3, t)] = [D_j(t; k, m), T_j(t; k, m), F_j(t; k, m)]\, e^{i(kx_1 + mx_3)}.$$

The 3-D formulation of the viscoelastodynamic relations (12)–(14) is then obtained by a simple rotation about the x_2-axis (see Fig. 3 in Geubelle and Rice (1995) for details). Unlike in the bimaterial case characterized by an intrinsic combination of the three fracture modes (Breitenfeld and Geubelle, 1997), the present homogeneous situation presents a decoupling between the tensile mode (Mode I), which generates a crack opening displacement in the x_2-direction only ($\delta_2 \neq 0, \delta_1 = \delta_3 = 0$), and the shear-dominated modes (Modes II and III) which create displacement discontinuities parallel to the crack plane (δ_1 and $\delta_3 \neq 0, \delta_2 = 0$). Following the procedure delineated in Geubelle and Rice (1995), the 3-D spectral displacement-based formulation in the viscoelastic tensile case is, for the SLS class of materials,

$$\tau_2(x_1, x_3, t) = \tau_2^0(x_1, x_3, t) - \frac{\mu_0 h}{2c_{s0}}\dot{\delta}_2(x_1, x_3, t) + \frac{\mu_0 \xi h}{4c_{s0}\tilde{\tau}}\delta_2(x_1, x_3, t) + f_2(x_1, x_3, t), \quad (17)$$

where

$$F_2(t; k, m) = -\frac{\mu_0 q}{2}\int_{-\infty}^{t} C_1^{VE}(qc_{s0}t')D_2(t-t'; k, m)qc_{s0}\,\mathrm{d}t',$$

$$F_2(t; 0, 0) = -h\frac{\mu_0}{2c_{s0}\tilde{\tau}}\int_{-\infty}^{t} C_0^{VE}\left(\frac{t'}{\tilde{\tau}}\right)D_2(t-t'; 0, 0)\frac{\mathrm{d}t'}{\tilde{\tau}}, \quad (18)$$

with $q = \sqrt{k^2+m^2}$, C_1^{VE} given in Appendix B and C_0^{VE} expressed in (11).

In the shear case, the 3-D spectral formulation becomes

$$\tau_j(x_1, x_3, t) = \tau_j^0(x_1, x_3, t) - \frac{\mu_0}{2c_{s0}}\dot{\delta}_j(x_1, x_3, t) + \frac{\mu_0 \xi}{4c_{s0}\tilde{\tau}}\delta_j(x_1, x_3, t) + f_j(x_1, x_3, t), \quad (j = 1 \text{ and } 3) \tag{19}$$

with

$$\begin{Bmatrix} F_1(t;k,m) \\ F_3(t;k,m) \end{Bmatrix} = -\frac{\mu_0}{2q}\begin{bmatrix} k^2 & km \\ km & k^2 \end{bmatrix}\int_{-\infty}^{t} C_{II}^{VE}(qc_{s0}t') \begin{Bmatrix} D_1(t-t';k,m) \\ D_3(t-t';k,m) \end{Bmatrix} qc_{s0}\,dt' - \frac{\mu_0}{2q}\begin{bmatrix} m^2 & -km \\ -km & m^2 \end{bmatrix}\int_{-\infty}^{t} C_{III}^{VE}(qc_{s0}t') \begin{Bmatrix} D_1(t-t';k,m) \\ D_3(t-t';k,m) \end{Bmatrix} qc_{s0}\,dt',$$

$$F_j(t;0,0) = -\frac{\mu_0}{2c_{s0}\tilde{\tau}}\int_{-\infty}^{t} C_0^{VE}\left(\frac{t'}{\tilde{\tau}}\right) D_j(t-t';0,0)\frac{dt'}{\tilde{\tau}}, \quad (j = 1 \text{ and } 3), \tag{20}$$

where the two convolution kernels C_{II}^{VE} and C_{III}^{VE} are also listed in Appendix B. The implementation of the spectral scheme is identical to that of the elastic case (Geubelle and Rice, 1995): a rectangular portion ($0 \leqslant x_1 \leqslant X; 0 \leqslant x_3 \leqslant Z$) of the fracture plane is discretized by a K^*M uniform grid on which the 2-D Fourier series is defined:

$$[\tau_j, \delta_j, f_j] = \sum_{k=-K/2}^{K/2}\sum_{m=-M/2}^{M/2}[T_j^{km}(t), D_j^{km}(t), F_j^{km}(t)]\exp\left[2\pi i\left\{\frac{kx_1}{X} + \frac{mx_3}{Z}\right\}\right].$$

The Fourier coefficients are computed efficiently by a 2-D Fast Fourier Transform scheme. Note that the computationally most expensive operation, the convolution over the past COD history, is described by (18) and (20) for each individual spectral mode (k, m), independently from the others. This unique aspect makes the spectral scheme particularly attractive in a massively parallel computing environment, especially for distributed memory architectures such as the CM-5 used in the present analysis; each spectral mode is assigned to one processor and the inter-processor communication is limited to a minimum.

To complete the numerical scheme, two relations are still needed: Firstly, a time stepping scheme must be used to obtain the displacement distribution from the velocity solution. In the displacement formulation used in the remainder of this paper, we use a simple and efficient explicit scheme

$$\delta_j(x_1, x_3, t+\Delta t) = \delta_j(x_1, x_3, t) + \Delta t \quad \dot{\delta}_j(x_1, x_3, t),$$

where the crack opening velocity $\dot{\delta}_j$ is derived from (17) in the tensile case and (19) in the shear situation. Secondly, a failure model must be introduced to simulate spontaneous crack growth. The numerical scheme allows for a wide range of cohesive and/or friction models: a simple rate-independent cohesive model was used in the Mode III viscoelastic case (Geubelle *et al.*, 1998). In the last section of this paper, rate-dependence is incorporated in the cohesive model in an analysis of spontaneous crack propagation of 2-D tensile cracks. The implementation of the spectral scheme in the 3-D situation is very similar to that described in the aforementioned 2-D Mode III paper and will not be repeated here.

The remainder of this paper presents some typical 2-D and 3-D applications of the viscoelastodynamic spectral scheme under tensile (Mode I) loadings [eqns (17) and (18)], starting with the classical 2-D problem of a tensile line load suddenly applied on a viscoelastic SLS half space.

3. TENSILE LINE LOAD ON A VISCOELASTIC HALF SPACE

The existence and properties of Rayleigh waves in viscoelastic materials have been the focus of various investigations over the past decades: through a detailed analysis of the dispersion relation in the viscoelastic case, Currie *et al.* (1977) and Currie and O'Leary (1978) have suggested that the surface waves appearing in viscoelastic media may be quite different from their elastic counterparts. The main difference pertains to the possible appearance of two surface waves: a quasi-elastic wave, traveling at a speed similar to that of the elastic Rayleigh wave (i.e., slower than both the dilatational and shear waves), and a purely viscoelastic wave, the speed of which may exceed that of the dilatational wave. These purely viscoelastic waves were shown, however, to be incompatible with additional physically motivated criteria associated with the behavior of harmonic surface waves at infinity (Ivanov and Savoya, 1993).

In the first application of the spectral scheme, we investigate viscoelastic effects on the propagation of transient surface waves generated by a tensile line load suddenly applied on an SLS half space. This classical problem constitutes a numerically challenging test for the spectral scheme since it is characterized by a highly concentrated applied load with non-vanishing spectral content, by the presence of very different wave effects and, under certain conditions, of singular velocity solutions. A portion X of the free surface is discretized by 1024 equally spaced grid points and a step point-load F is suddenly applied at $t = 0$ in the middle of the domain of interest. The constant Poisson's ratio ν is chosen as 0.25 and the modulus ratio ξ as 1 (i.e., $\mu_\infty = \mu_0/2$). To illustrate the transient viscoelastodynamic effects, the evolution of the vertical velocity $\dot{u}_2$ of a surface point located at a distance L from the point of application of the line load is presented in Fig. 4 for the elastic case (solid curve) and five values of $c_{s0}\tilde{\tau}$ (dashed curves). As expected, for large values of the relaxation time, the material behaves almost elastically and the numerical values follow the analytical (Lamb) solution characterized by a small downward motion at the arrival of the dilatational wave ($t = L/c_{d0}$), a change of slope at the arrival of the shear wave ($t = L/c_{s0}$) and a strong singularity associated with the Rayleigh wave ($t = 1.088L/c_{s0}$). The small spurious oscillations appearing before the arrival of the dilatational wave are due to the non-vanishing spectral content of the spatially concentrated load (Geubelle and Rice, 1995).

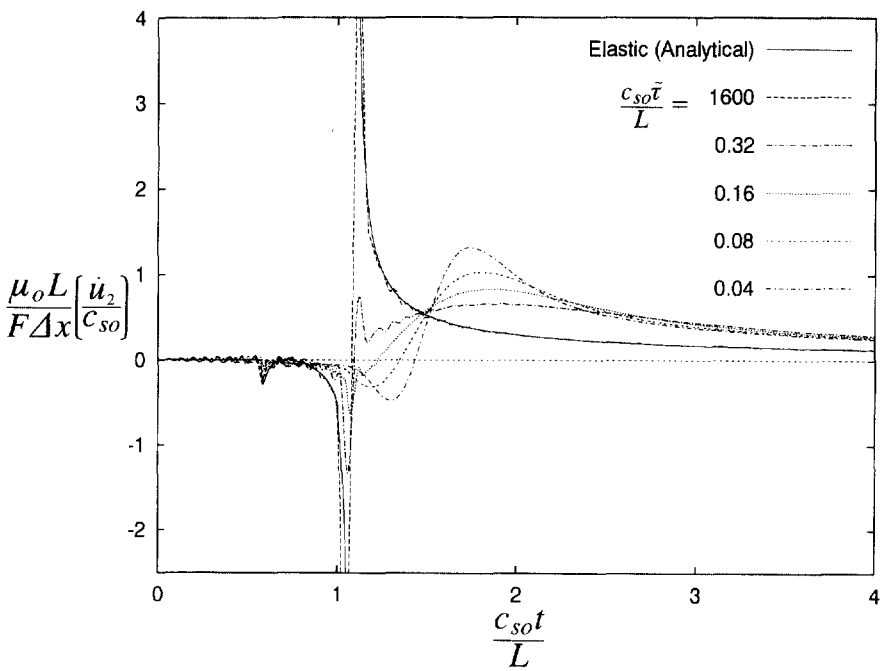

Fig. 4. Tensile line load on a viscoelastic half-space: normal velocity response u_2 observed at a point located at a distance L from the point of application of the load P, illustrating the effect of the relaxation time $\tilde{\tau}$ on the propagation of surface waves.

As the ratio $c_{s0}\tilde{\tau}/L$ of elastodynamic to viscoelastic time scales increases, the material relaxation starts to play a more prominent role and strongly affects the motion of the free surface. The most striking effect is associated with the damping of the singularity of the Rayleigh wave, the arrival of which is shifted progressively to later times. In the limiting case $c_{s0}\tilde{\tau} \to 0$, the surface wave propagation will take place essentially in a fully relaxed medium, and the Rayleigh wave will regain its "elastic singularity", as indicated by the trend shown in Fig. 4. For the material combination used here ($\xi = 1$ and $\nu = 0.25$), its arrival time will then be $c_{s0}t/L \approx 1.538$. Finally, note the larger long-time velocity also characteristic of the drop in elastic moduli.

4. SUDDEN TENSILE LOADING OF AN ELLIPTICAL CRACK

The classical 3-D problem of the sudden uniform Mode I loading of a stationary elliptical crack embedded in a viscoelastic medium is now investigated. A square portion ($X = Z$) of the fracture plane is discretized by a uniform $512 * 512$ grid. The elliptical crack is located at the center of the domain of interest, with the major axis parallel to the x_1-axis. It has an aspect ratio of 3/2 and its major and minor axes are discretized by 192 and 128 grid spacings, respectively. The pre-existing crack is prevented from propagating by assigning a very high strength to the surrounding viscoelastic medium. The simulations were performed using the SLS model, with a modulus ratio parameter $\xi = 1$. As was the case in the previous section, the time step size Δt was chosen as $\Delta x/2c_{s0}$, where Δx denotes the grid spacing.

The evolution of the crack opening displacement (COD) along the major axis ($x_3 = Z/2$) of the elliptical crack is shown in Fig. 5(a) for the elastic case, and in Fig. 5(b) and (c) for two viscoelastic situations with $c_{s0}\tilde{\tau}/X = 0.5$ and 0.05, respectively. All three cases present the overshoot characteristic of dynamic fracture problems: the COD reaches a peak before settling down to the long time ellipsoidal deformed shape. The intensity of the dynamic overshoot (i.e., the ratio of the peak value to the long-term one) is, however, stronger in the elastic situation. As expected, since most of the complex transient effects are associated with the propagation of Rayleigh waves along the crack surfaces, the reflecting sharp wave fronts and the oscillations apparent in the elastic case (Fig. 5(a)) quickly disappear in the viscoelastic cases which present a smoother surface, especially in the fully relaxed situation (Fig. 5(c)) where very little wave propagation can be detected. The first viscoelastic case (Fig. 5(b)) presents an intermediate situation for which the viscous effect starts to play a major role after the first Rayleigh wave reflection. The transient effects are then quickly damped out and the deformed crack shapes slowly approach the fully relaxed limit.

The damping effect of the surrounding viscoelastic medium on the transient waves propagating along the fracture surface can be better illustrated in Fig. 6, which presents the evolution of the crack opening velocity $\dot{\delta}_2$ computed at the center of a 2-D non-moving crack of length $2a$ suddenly subjected to a uniform tensile loading. The properties of the surrounding material are identical to those used in the 3-D problem described earlier. The elastic case (solid curve) is characterized by a constant velocity until the arrival of the dilatational wave, followed by the shear wave and the singular Rayleigh wave. After this initial train of waves, the crack opening velocity quickly drops and oscillates around zero until the quasi-static limit is achieved. For fairly large values of the relaxation time parameter $\tilde{\tau}$ ($c_{s0}\tilde{\tau}/2a \geqslant 2$), the arrival of these waves is felt in a similar way. However, material relaxation tends to damp their effect, especially after the second wave reflections from the crack ends. For small values of $\tilde{\tau}(c_{s0}\tilde{\tau}/2a \leqslant 0.2)$, the material relaxes before the arrival of the first Rayleigh wave and the velocity response is much "smoother". Note once again the shift of the time of arrival and the damping of the Rayleigh wave already mentioned in the previous section.

5. PROPAGATING MODE I CRACK

In this final section, we present the results of a series of simulations of spontaneous crack propagation and arrest in elastic and viscoelastic media under tensile loading

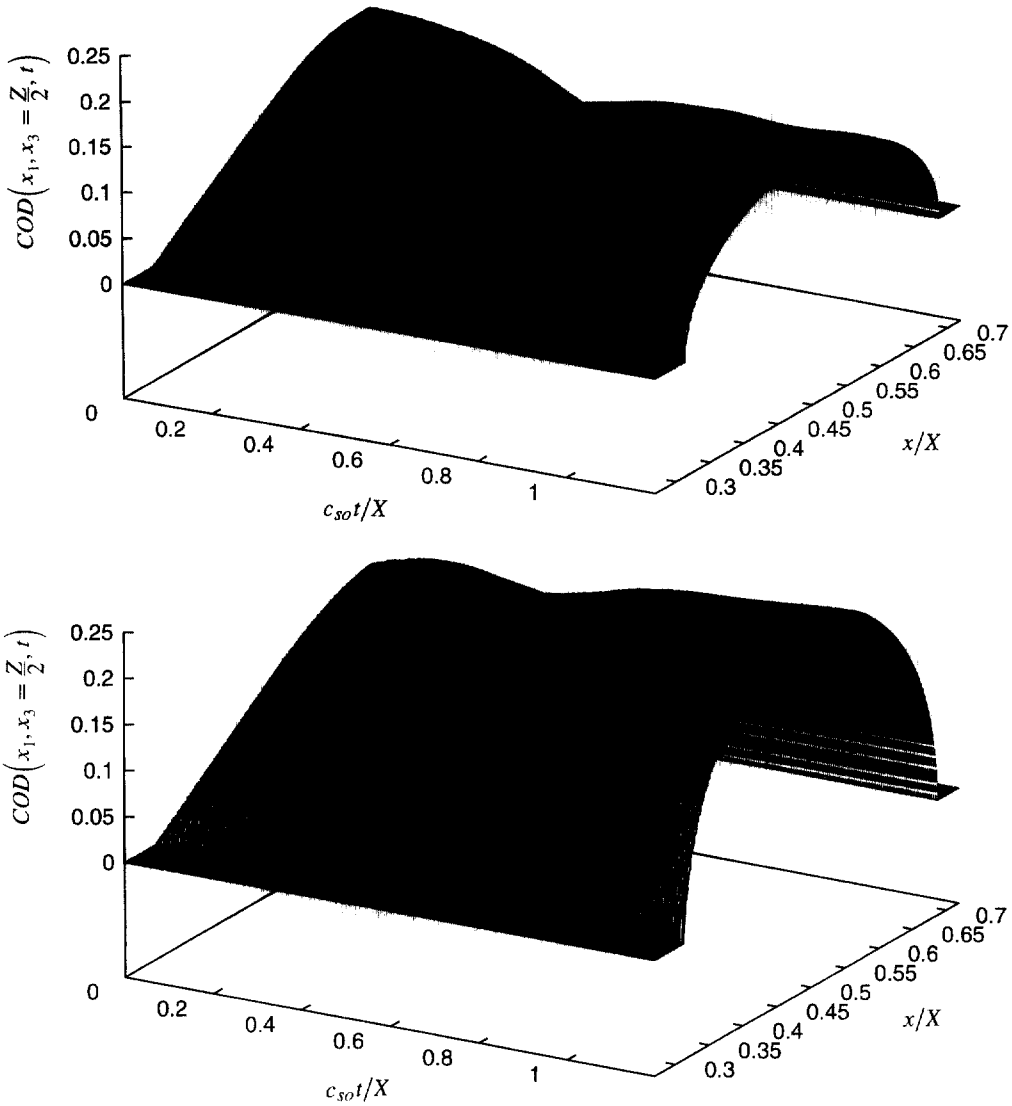

Fig. 5. Evolution of the crack opening displacement along the major axis of a stationary elliptical crack subjected to a sudden uniform tensile loading in the elastic case (a), for $c_{s0}\tilde{t}/X = 0.5$ (b), and for $c_{s0}\tilde{t}/X = 0.05$ (c), showing the viscoelastic effect on the dynamic overshoot.

conditions. Of particular interest hereafter is the effect of the rate-dependence of the cohesive failure model on the crack motion. The role of cohesive failure in dynamic fracture, especially within the context of the spontaneous propagation of fast cracks, is a complex and still poorly understood issue. Recently, Yang and Ravi-Chandar (1996) have performed a detailed finite different analysis of the role of cohesive failure in the steady-state and unsteady motion of Mode III cracks in linearly elastic materials. The cohesive model used in their simulations involved a thin layer of uniform thickness placed ahead of the crack and characterized by a rate-independent strain-based progressive failure model. They emphasized in their conclusion the primordial role that the cohesive model plays on the spontaneous crack motion. The preliminary investigation presented in this section aims at complementing their work by introducing rate dependence in the failure model. The evolution of the process zone for rapidly propagating cracks has also been the subject of another numerical analysis by Johnson (1992) who used a simple cell model to characterize the weakening behavior of the material in the process zone. Also related to the issue of process zone modeling are the papers by Gurtin (1979) and Costanzo and Allen (1995), which

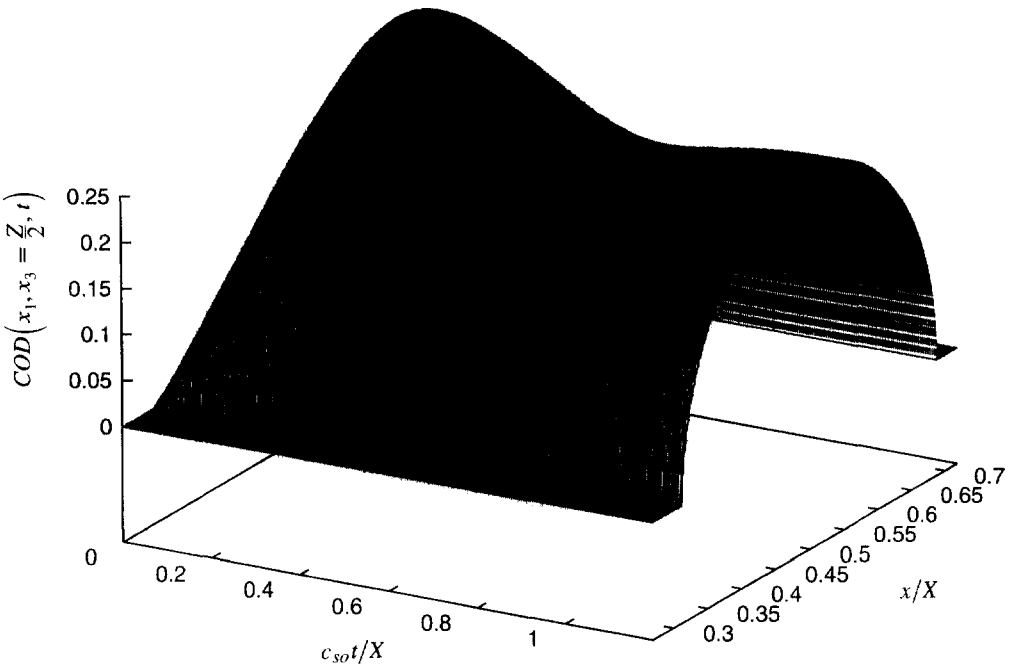

Fig. 5.—*Continued.*

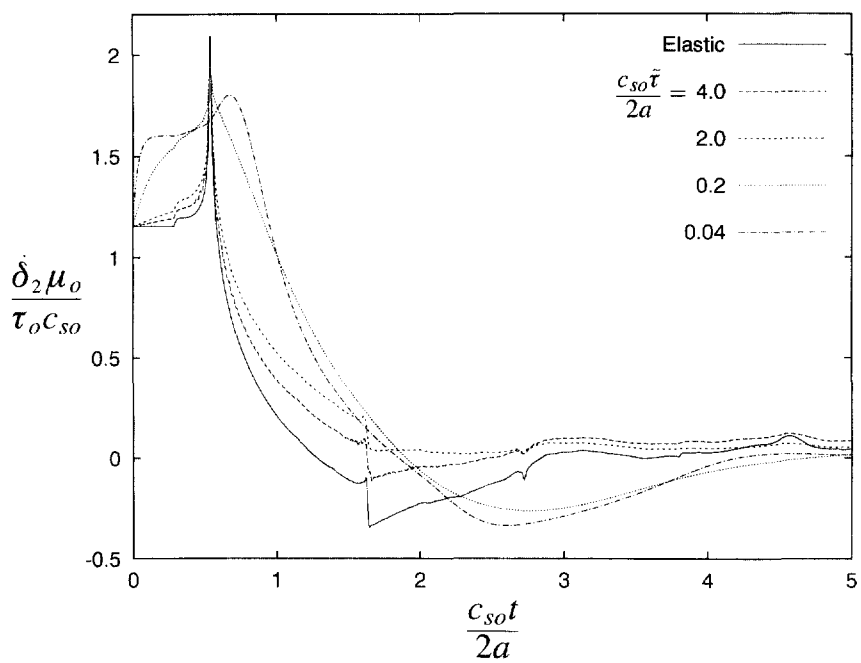

Fig. 6. Evolution of the crack opening velocity $\dot{\delta}_2$ at the center of a 2-D crack of length $2a$ subjected to a sudden uniform pressure τ_0.

present a thermodynamics-based theoretical framework for elastic and viscoelastic cohesive zone models.

As indicated earlier, the spectral scheme allows for the incorporation of a wide range of cohesive models to characterize the failure process. In the preliminary Mode III paper (Geubelle *et al.*, 1998), the authors have shown how the viscoelastic behavior of the

surrounding medium affects the limiting speed of a crack subjected to anti-plane shear loading conditions. In order to focus on the viscoelastic effect of the surrounding medium, the failure model was chosen as rate independent. The simple linear cohesive model used there is now extended to include a dependence on the crack opening velocity $\dot{\delta}_2$ as in

$$\tau_{\text{strength}} = \max\left\{\tau_c\left(1-\frac{\delta_2}{\delta_c}\right)\left(1+k\frac{|\dot{\delta}_2|}{c_{s0}}\right), 0\right\}, \tag{21}$$

where τ_c denotes the original ("intact") strength of the material, δ_c is the critical value of the crack opening displacement beyond which complete failure is assumed, and k is a non-dimensional parameter characterizing the rate-dependence of the cohesive failure process.

The failure model (21) is clearly very simple and is introduced here primarily for illustrative purposes. More complex nonlinear cohesive failure models have been proposed in the quasi-static case for viscoelastic materials, such as those used by Schapery (1975) and Knauss and Losi (1993).

The problem simulated hereafter involves a finite size crack of length $2a_0$ located at the center of a domain $X = 16a_0$ discretized by 2048 grid spacings. A uniform constant tensile load τ_0 is suddenly applied along the pre-existing crack as

$$\tau_2^0(x_1, t) = \tau_0 H(t) H\left(x_1 - \frac{X}{2} + a_0\right) H\left(\frac{X}{2} + a_0 - x_1\right),$$

where H denotes the Heaviside function. The load amplitude τ_0 is chosen equal to the initial strength τ_c of the surrounding medium, while the critical crack opening displacement $\delta_c = 0.03$. The time step is chosen as $c_{s0}\Delta t = \Delta x/4$. Special care was taken in all simulations to discretize the cohesive zone with at least 25 elements to capture with great precision the failure process described by (21).

Due to the sudden loading of the crack faces, a stress concentration builds up in the vicinity of the crack tips, leading to the progressive failure of the adjacent material on the fracture plane. The evolution of the deformed crack shape is presented in Fig. 7 for the

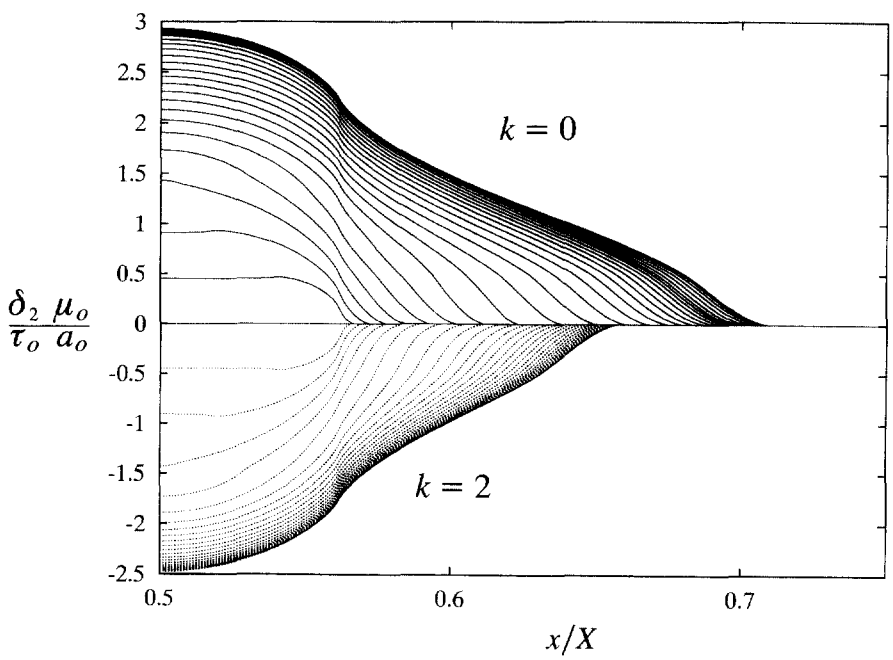

Fig. 7. Effect of the rate-dependence of the cohesive failure model on the crack opening displacement profile for a Mode I crack propagating spontaneously in a linearly elastic material. The rate-dependent case ($k = 2$) is presented inverted with respect to the horizontal axis for clarity purposes. Each curve is separated by 200 time steps.

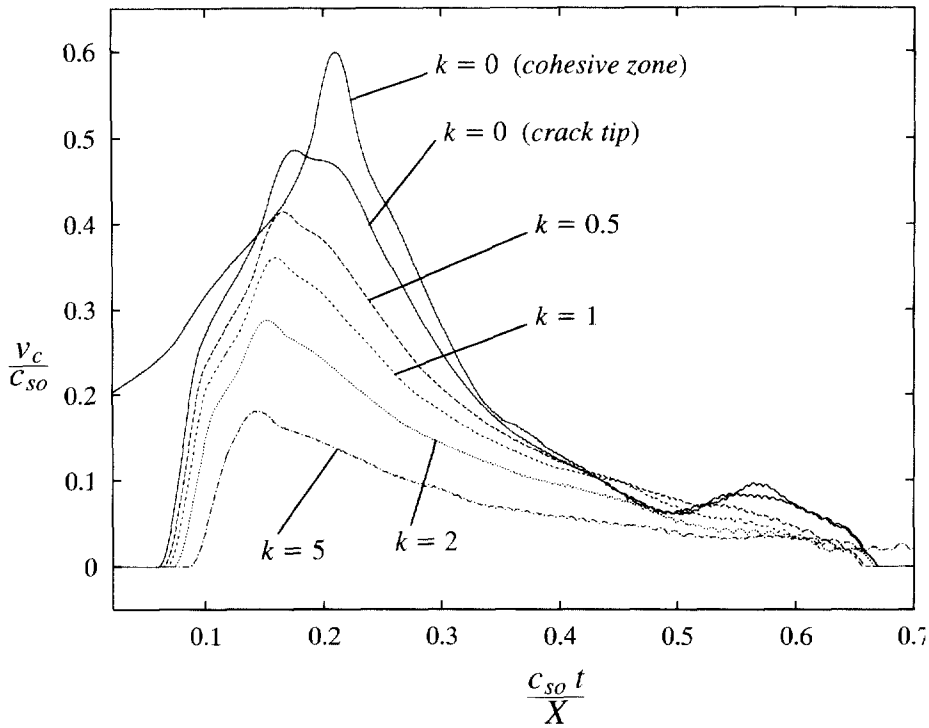

Fig. 8. Evolution of the crack tip velocity in the elastic case for various values of k. The evolution of the tip of the cohesive zone is also indicated for the rate-independent situation ($k = 0$).

elastic situation ($c_{s0}\tilde{\tau} \to \infty$) with $k = 0$ (solid curve) and $k = 2$ (dashed curve). The time interval $\bar{T}$ between successive curves corresponds to 200 time steps, i.e., $c_{s0}\bar{T} \simeq 0.4a_0$. Taking advantage of the symmetry of the problem, only the right half of the crack is shown, emphasizing the cusp-like shape of the opened crack, a feature characteristic of cohesive failure.

As indicated by the spacing between the successive curves, the crack goes through an acceleration phase before slowing down and eventually arresting. This unsteady motion is illustrated in Fig. 8, which presents the evolution of the velocity of the crack tip and cohesive zone tip for various values of k in the elastic situation. The oscillations appearing at the end of the simulations are associated with the numerical differentiation of very slowly advancing crack fronts. For the sake of clarity, the velocity of the tip of the cohesive zone (i.e., the right-most point with non-zero crack opening displacement) is only presented for the rate-independent situation ($k = 0$), but its evolution is representative of all simulations: as expected, the cohesive zone tip starts to propagate almost immediately, while the actual crack tip (the right-most point for which $\delta_2 \geqslant \delta_c$) remains stationary until sufficient crack opening is achieved. Then, as observed experimentally (Ravi-Chandar and Knauss, 1984), the crack tip accelerates very quickly in an attempt to "catch up" with the tip of the cohesive zone.

As shown in Figs 7 and 8, the rate dependence of the failure process has a strong effect on the maximum crack speed and on the extent of crack advance. This is to be expected as the rate-dependent term in (21) creates an additional energy release mechanism. This fact is further illustrated in Fig. 9, which presents the evolution of the energy $\dot{W}$ released in the failure process and defined by

$$\dot{W}(t) = \int_{\text{coh. zone}(t)} \tau_{\text{strength}}(x_1, t)\dot{\delta}_2(x_1, t)\, \mathrm{d}x_1.$$

The energy rate is normalized by $c_{s0}G_c = 2c_{s0}/\tau_c\delta_c$, which represents the rate of energy that

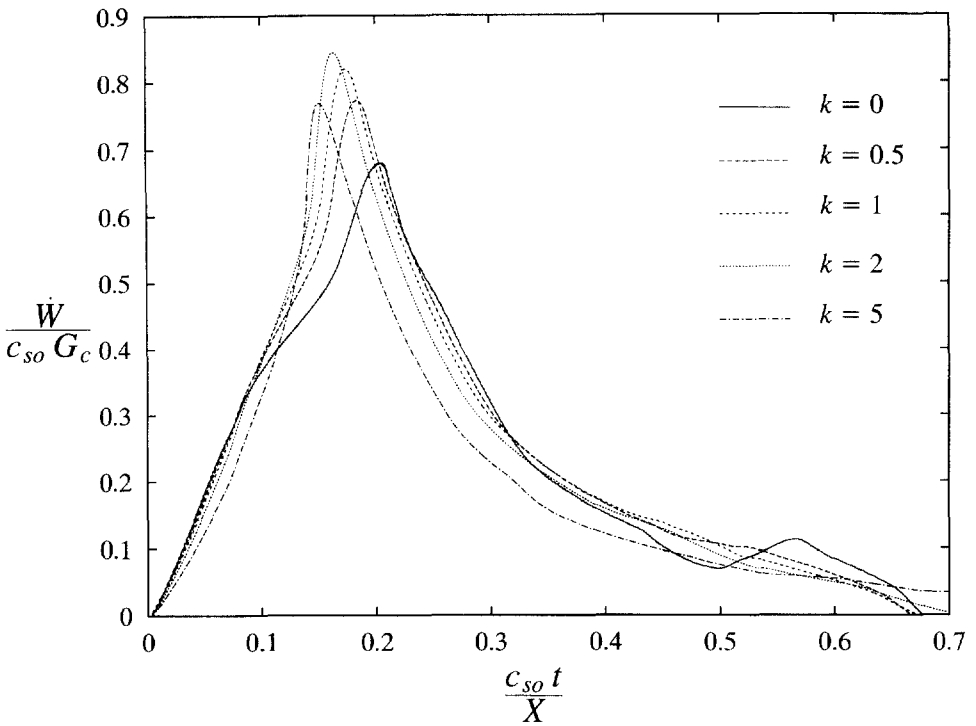

Fig. 9. Effect of k on the rate of energy $\dot{W}$ dissipated in the cohesive failure process described in Figs 7 and 8.

would be dissipated by a tensile crack propagating steadily at velocity c_{s0} in a material characterized by a rate-independent linear cohesive model [eqn (21) with $k = 0$]. As indicated in Fig. 9, the rate of energy first increases, reaches a maximum and then progressively decreases with k. This non-monotonic behavior can be explained by the two opposing effects k has on the energy dissipation mechanism: it increases $\dot{W}$ by introducing an additional "viscous" term, but also reduces the crack velocity, and thereby the rate at which energy is dissipated.

The rate dependence of the failure process can also be observed in the evolution of the crack opening velocity $\dot{\delta}_2$ at a point located at a distance $3a_0/4$ from the initial location of the crack tip (Fig. 10). As expected, the peak opening velocity decreases with k due to the combined effects of a decreasing crack velocity and the increasing importance of the viscous term. It is also interesting to note how the introduction of rate dependence in the cohesive failure model "stabilizes" the numerical scheme by absorbing the spurious dynamic effects associated with the step-like advance of the crack front.

Unsurprisingly, many observations obtained in the elastic case are reproduced in the viscoelastic situation. It is clear that the importance of the viscoelastic behavior of the surrounding medium depends on the relative value of the relaxation time $\tilde{\tau}$ compared to a characteristic elastodynamic time of the dynamic fracture problem, defined, for example, as the time needed for a shear wave to travel along the initial crack. In the following example, we chose $c_{s0}\tilde{\tau}/a_0 = 1.6$ to emphasize the viscoelastic effect. The modulus ratio ξ was taken as unity. All the other variables (initial crack length, strength, applied load, ...) are the same as in the elastic case described above.

As indicated in the evolution of the crack opening profile (Fig. 11), the relaxation of the surrounding viscoelastic medium affects the spontaneous motion of the Mode I crack in two ways: firstly, while the crack goes through a similar acceleration and deceleration phase, its peak velocity value is less in the viscoelastic situation than in the elastic case, as is apparent from the maximum spacing between the successive curves. Secondly, because of the relaxation of the surrounding medium, larger crack opening displacement is achieved

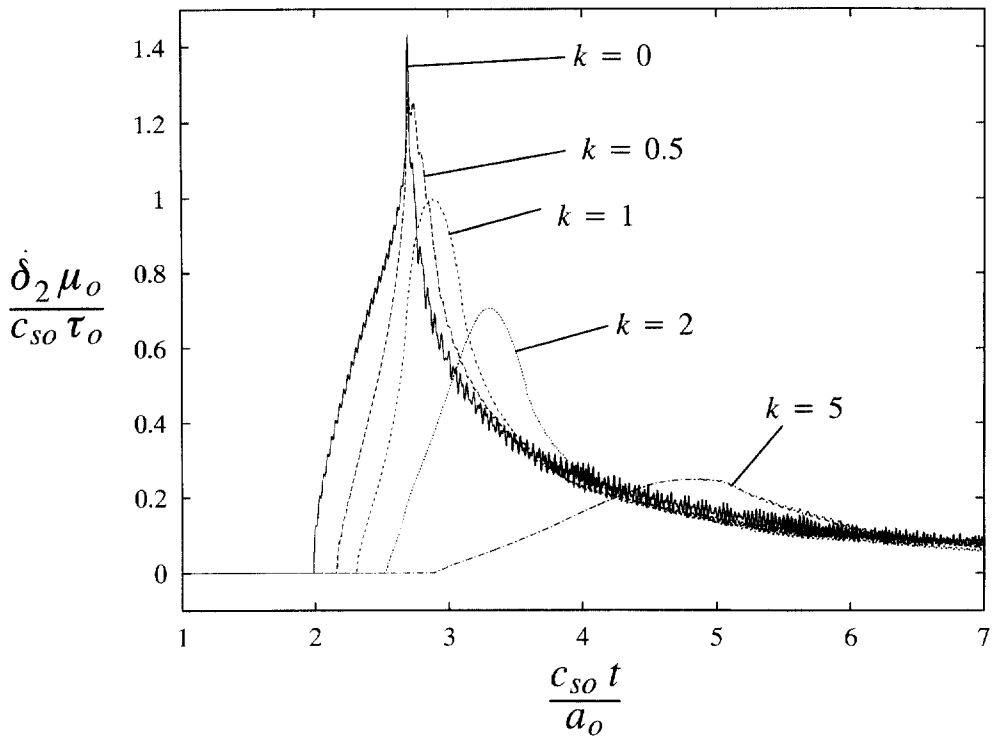

Fig. 10. Pointwise crack opening velocity $\dot{\delta}_2$ observed at a point located at a distance $3a_0/4$ ahead of the initial crack tip in the elastic case for various values of k.

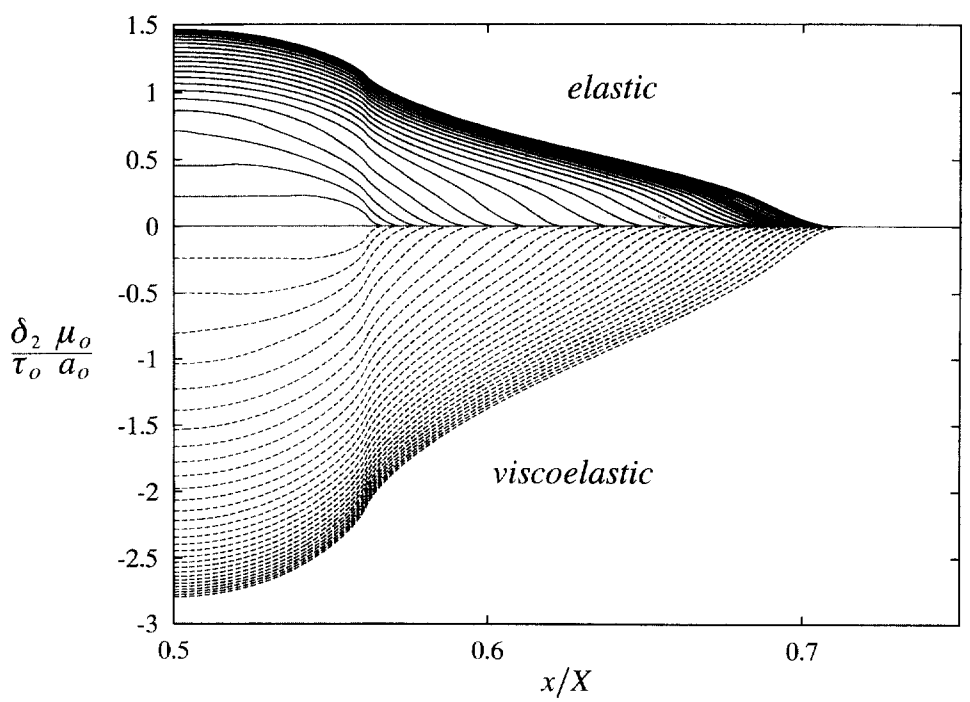

Fig. 11. Comparison between the crack opening profile observed in the elastic (solid curve) and viscoelastic (dashed curve) problems for a rate-independent cohesive failure model.

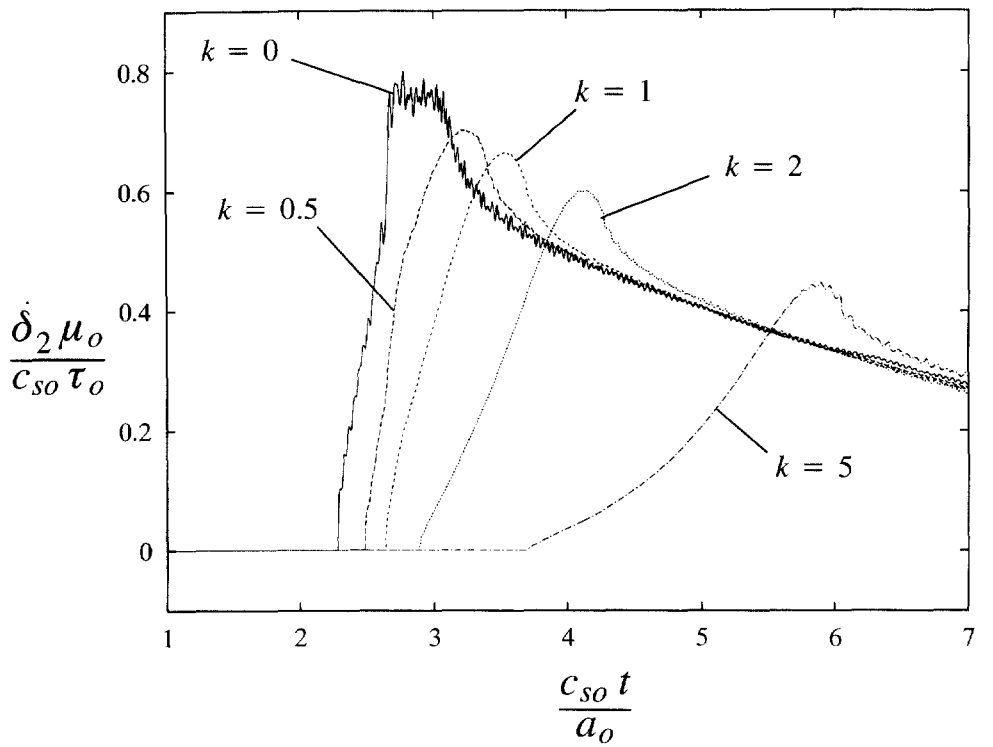

Fig. 12. Pointwise crack opening velocity $\dot{\delta}_2$ of a point located at a distance $3a_0/4$ ahead of the initial crack tip in the viscoelastic case.

in the viscoelastic case, leading to additional energy available for fracture and, therefore, to increased crack extension. The effect of the rate dependence of the cohesive failure model on the pointwise crack opening velocity (Fig. 12) is somewhat similar to that observed in the elastic situation. The decrease in peak opening velocity with increasing values of k is, however, less dramatic, as the viscous response of the surrounding viscoelastic medium prevents the appearance of high opening rates. This effect is especially apparent in the rate-independent situation ($k = 0$) : while a singular opening velocity was observed at the passage of the crack tip (i.e., the end of the cohesive zone) in the elastic case (Fig. 10), the crack opening velocity is clearly limited to a finite value in the viscoelastic situation (Fig. 12).

The results presented in this section have only shed some light on the important role rate dependence plays in dynamic cohesive failure and motivate the need for additional analytical and numerical work on the topic. This more detailed analysis is, however, beyond the scope of this paper and will be the subject of our future investigations.

6. CONCLUSION

A numerical method based on a special form of the boundary integral formulation for 2-D and 3-D visco-elastodynamic problems has been presented. This numerical scheme is derived from an exact spectral representation of the relationship existing between the stresses and displacements existing on the fracture plane. The algorithm allows for the simulation of spontaneously propagating planar cracks and faults embedded in a viscoelastic material whose mechanical response is modeled with an arbitrary Prony series representation. The crack can be subjected to any dynamic loading conditions, and spontaneous crack propagation is achieved with the aid of a cohesive failure model of arbitrary complexity.

Through 2-D and 3-D simulations involving free surfaces and stationary cracks, the strong viscoelastic effects on the magnitude, shape and speed of surface waves, and on the dynamic overshoot have been described for the SLS model. A simple rate-dependent cohesive model has also been formulated and implemented to provide some insight on the influence of rate effects on the spontaneous propagation and arrest of cracks in an elastic and a viscoelastic medium.

Acknowledgement—The 3-D simulations presented in this paper have been performed on the CM-5, available at the National Center for Supercomputing Applications.

REFERENCES

Breitenfeld, M. S. and Geubelle, P. H. (1997) Numerical analysis of dynamic debonding under in-plane and 3-D loading conditions. *International Journal of Fracture*, submitted.

Costanzo, F. and Allen, D. H. (1995) A continuum thermodynamic analysis of cohesive zone models. *Int. J. Engng. Sci.* **33,** 2197–2219.

Crump, K. S. (1976) Numerical inversion of Laplace transforms using Fourier series approximation. *J. Assoc. Comp. Mach.* **23,** 89–96.

Currie, P. K. and O'Leary, P. M. (1978) Viscoelastic Rayleigh waves II. *Quart. Appl. Math.* **35,** 445–454.

Currie, P. K., Hayes, M. A. and O'Leary, P. M. (1977) Viscoelastic Rayleigh waves. *Quart. Appl. Math.* **35,** 35–53.

Dubner, H. and Abate, J. (1968) Numerical inversion of Laplace transforms by relating them to the finite Fourier cosine transform. *J. Assoc. Comp. Mach.* **15,** 115–123.

Duong, C. and Knauss, W. G. (1995) A nonlinear thermoviscoelastic stress and fracture analysis of an adhesive bond. *Journal of the Mechanics and Physics of Solids* **43,** 1505–1549.

Georgiadis, H. G. (1993) Shear and torsional impact of cracked viscoelastic bodies—A numerical integral equation/transform approach. *International Journal of Solids and Structures* **30,** 1891–1906.

Georgiadis, H. G., Theocaris, P. S. and Mouskos, S. C. (1991) Plane impact of a cracked viscoelastic body. *Int. J. Eng. Sci.* **29,** 171–177.

Geubelle, P. H. and Rice, J. R. (1995) A spectral method for three-dimensional elastodynamic fracture problems. *Journal of the Mechanics and Physics of Solids* **43,** 1791–1824.

Geubelle, P. H., Danyluk, M. J. and Hilton, H. H. (1998) Dynamic Mode III fracture in viscoelastic media. *International Journal of Solids and Structures*, **35,** 761–782.

Gurtin, M. E. (1979) Thermodynamics and cohesive zone in fracture. *J. Appl. Math. Physics (ZAMP)* **30,** 991–1003.

Hilton, H. H. (1996) On the inadmissibility of separation of variables solutions in linear anisotropic viscoelasticity. *Mech. Comp. Mater. Struct.* **3,** 97–100.

Hilton, H. H. and Yi, S. (1997) The significance of anisotropic viscoelastic Poisson ratio stress and time dependencies. UILU ENG 97-0503 Report, Univ. Illinois Urbana-Champaign. *International Journal of Solids and Structures*, in press.

Ivanov, TS. P. and Savova, R. (1993) Viscoelastic surface waves. *Eur. J. Mech., A/Solids* **12,** 667–677.

Johnson, E. (1992) Process region changes for rapidly propagating cracks. *International Journal of Fracture* **55,** 47–63.

Knauss, W. G. and Losi, G. U. (1993) Crack propagation in a nonlinearly viscoelastic solid with relevance to adhesive bond failure. *Journal of Applied Mechanics* **60,** 793–801.

Masuero, J. R. and Creus, G. J. (1993) Finite element analysis of viscoelastic fracture. *International Journal of Fracture* **60,** 267–282.

Ravi-Chandar, K. and Knauss, W. G. (1984) An experimental investigation into dynamic fracture: II. Microstructural aspects. *International Journal of Fracture* **26,** 65–80.

Schapery, R. A. (1975) A theory of crack initiation and growth in viscoelastic media III. Analysis of continuous growth. *International Journal of Fracture* **11,** 549–562.

Warby, M. K., Walton, J. R. and Whitman, J. R. (1992) A finite element model of crack growth in a finite body in the context of Mode I linear viscoelastic fracture. *Comp. Meth. Appl. Mech. Engr.* **97,** 375–397.

Yang, B. and Ravi-Chandar, K. (1996) On the role of the process zone in dynamic fracture. *Journal of the Mechanics and Physics of Solids* **44,** 1955–1976.

APPENDIX A

Starting with eqn (10), the last relations leading to the spectral formulation (12) are specific to the SLS class of viscoelastic materials with constant Poisson's ratio. In this first appendix, we extend this result to a general class of viscoelastic materials, for which the non-synchronous shear and bulk relaxation moduli are expressed through the conventional (but distinct) Prony series:

$$\mu(t) = \mu_\infty + \sum_{n=1}^{N_\mu} \mu_n e^{-t/\tau_n^\mu},$$

$$K(t) = K_\infty + \sum_{n=1}^{N_K} K_n e^{-t/\tau_n^K}, \tag{A1}$$

The Laplace transforms of the corresponding shear and bulk moduli are

$$\hat{\mathscr{H}}(p) = 1 - \sum_{n=1}^{N_S} \frac{\mu_n}{\mu_0 \tilde{\tau}_n^S} \frac{1}{p + 1/\tilde{\tau}_n^S},$$

$$\hat{\mathscr{K}}(p) = 1 - \sum_{n=1}^{N_K} \frac{K_n}{K_0 \tilde{\tau}_n^K} \frac{1}{p + 1/\tilde{\tau}_n^K}, \tag{A2}$$

where

$$\mu_0 = \mu_\infty + \sum_{n=1}^{N_S} \mu_n \quad \text{and} \quad K_0 = K_\infty + \sum_{n=1}^{N_K} K_n$$

are the instantaneous elastic shear and bulk moduli, respectively. The auxiliary operator $\hat{\mathscr{Q}}$ appearing in (3) and (5) is related to $\hat{\mathscr{K}}$ and $\hat{\mathscr{H}}$ through

$$\hat{\mathscr{Q}}(p) = \gamma_0 \hat{\mathscr{K}}(p) + (1 - \gamma_0) \hat{\mathscr{H}}(p), \tag{A3}$$

where

$$\gamma_0 = \frac{K_0}{K_0 + \frac{4}{3}\mu_0}.$$

Substituting (A2) and (A3) into the square bracketed terms in (7), we obtain the general form of $R_z^{VE}(T)$. After some algebraic manipulations, we can extract the limiting values

$$R_1^\infty = -\frac{1}{|q| c_{s0} \tilde{\tau}^*} \eta_1,$$

$$R_2^\infty = -\frac{h}{|q| c_{s0} \tilde{\tau}^*} \eta_2,$$

where $h = c_{d0}/c_{s0}$ and η_α are non-dimensional material parameters

$$\eta_1 = \frac{1}{2} \sum_{n=1}^{N_S} \frac{\mu_n}{\mu_0} \frac{\tilde{\tau}^*}{\tilde{\tau}_n^S},$$

$$\eta_2 = \frac{1}{2} \left[\gamma_0 \sum_{n=1}^{N_K} \frac{K_n}{K_0} \frac{\tilde{\tau}^*}{\tilde{\tau}_n^K} + (1 - \gamma_0) \sum_{n=1}^{N_S} \frac{\mu_n}{\mu_0} \frac{\tilde{\tau}^*}{\tilde{\tau}_n^S} \right], \tag{A4}$$

in which $\tilde{\tau}^*$ is an arbitrarily chosen representative relaxation time.

The final spectral form (12) of the viscoelastodynamic equations obtained for the SLS class of viscoelastic materials is thus also valid for this general class of materials described by (A1), provided that the diagonal matrix W_{ij} is written as

$$[W_{ij}] = \frac{\mu_0}{2 c_{s0} \tilde{\tau}^*} \operatorname{diag} [\eta_1, h\eta_2, \eta_1]. \tag{A5}$$

Relation (13) obtained in the text for the special SLS class of viscoelastic materials can be recovered from (A4) and (A5) by imposing $N_S = N_K = 1$, $\tau_1^S = \tilde{\tau}_1^K = \tilde{\tau}/(1+\xi)$, $\tilde{\tau}^* = \tilde{\tau}$, and $K_1/K_0 = \mu_1/\mu_0 = \xi/(1+\xi)$.

APPENDIX B

The convolution kernels for the displacement-based viscoelastodynamic spectral formulation using the SLS model are given in the Laplace domain by

$$\hat{C}_{\mathrm{I}}^{VE}(s) = \hat{C}_{2}^{VE}(s) = \frac{-4(s+b)^2\sqrt{1+s^2\left(\frac{s+b+b\xi}{s+b}\right)}}{s^2(s+b+b\xi)^2} + \frac{(s+b)^2\left[2+s^2\left(\frac{s+b+b\xi}{s+b}\right)\right]^2}{s^2(s+b+b\xi)^2\sqrt{1+\left(\frac{s}{h}\right)^2\left(\frac{s+b+b\xi}{s+b}\right)}} - hs + \frac{hb\xi}{2},$$

$$\hat{C}_{\mathrm{II}}^{VE}(s) = \hat{C}_{1}^{VE}(s) = \frac{-4(s+b)^2\sqrt{1+\left(\frac{s}{h}\right)^2\left(\frac{s+b+b\xi}{s+b}\right)}}{s^2(s+b+b\xi)^2} + \frac{(s+b)^2\left[2+s^2\left(\frac{s+b+b\xi}{s+b}\right)\right]^2}{s^2(s+b+b\xi)^2\sqrt{1+s^2\left(\frac{s+b+b\xi}{s+b}\right)}} - s + \frac{b\xi}{2}.$$

For reference, the Mode III kernel is given by (Geubelle *et al.*, 1998)

$$\hat{C}_{\mathrm{III}}^{VE}(s) = \hat{C}_{3}^{VE}(s) = \sqrt{1+s^2\left(1+\frac{b\xi}{s+b}\right)}\left(\frac{s+b}{s+b+b\xi}\right) - s + \frac{b\xi}{2}.$$